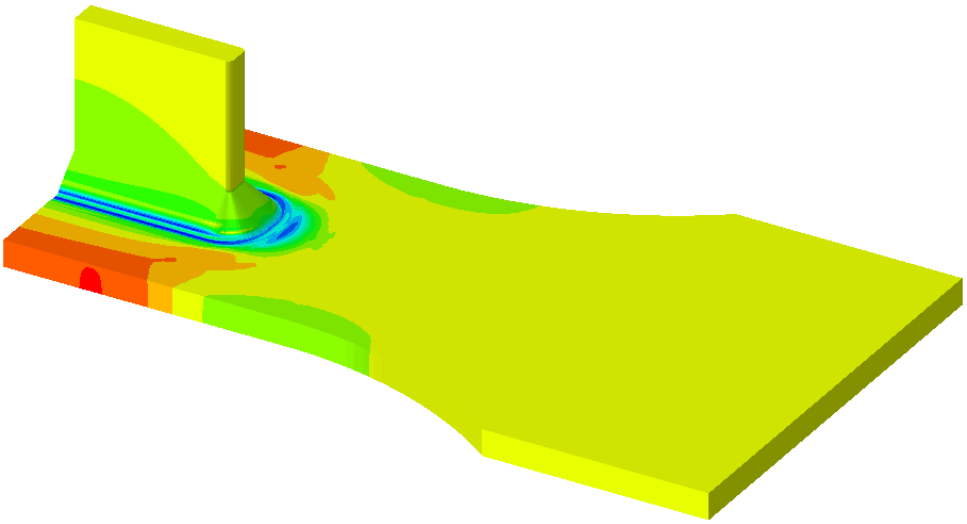

High frequency mechanical impact treatment to improve fatigue life of welds

Research report - Department of Mechanics and Maritime Sciences
2018:03
Project in Applied Mechanics 2018

Authors
Rikard Berg
Adam Billberg
Felix Eriksson
Ingrid Lövgren
Joel Nilsson
Mayur Sudarshan Rao

Supervisors
Lennart Josefson
Moyra McDill

Department of Mechanics and Maritime Sciences
Chalmers University of Technology
Göteborg, Sweden 2018

High frequency mechanical impact treatment to improve fatigue life of welds

Project in Applied Mechanics 2018

Research report - Department of Mechanics and Maritime Sciences 2018:03

Department of Mechanics and Maritime Sciences
Chalmers University of Technology
SE-412 96 Göteborg
Telephone +46 (0)31 772 1000

Preface

The work in the present report was carried out as a part of the course TME131 Project in Applied Mechanics, which is a mandatory course within the Applied Mechanics Masters programme at Chalmers. The course was carried out during spring semester 2018.

Acknowledgements

The project group would like to thank Prof. Em. Moyra McDill (Carleton University) and Prof. Lennart Josefsson (Chalmers University of Technology), for their guidance and support throughout the project.

In addition we would like to thank Jakob Alm who provided us with an introduction to Abaqus and other usefull information that has proved a great asset during our work.

Abstract

High frequency mechanical impact (HFMI) is a post-weld peening process which is carried out to improve the fatigue life of welded geometries. The increase in fatigue strength is attributed to the combination of inducing compressive residual stresses at the weld toe, a change in the weld toe geometry from the peening, as well as an increased surface hardness in the treated region. To further investigate the beneficial effects of HFMI, a benchmark exercise has been developed in the Specialist Committee V.3 Materials and Fabrication Technology of the International Ship and Offshore Structures Congress (ISSC 2018). The eventual expectation is the development of design guidelines for the use of HFMI in cyclically loaded components found, for example, in the ship building industry.

The benchmark exercise specifies the use of S355, a structural steel with a minimum yield strength of 355 MPa, and a particular coupon geometry, which consists of a stiffener, fillet welded to a membrane loaded plate. This geometry, provided as a finite element model by the benchmark exercise committee, is known to be sensitive to fatigue as it has a high stress concentration at the weld toe. Material and mechanical properties for the simulation of HFMI and the cyclic analysis are also specified. Chalmers University of Technology contributes to the benchmark exercise through the course TME131 – Project in applied mechanics.

In this year's project, an efficient way of simulating HFMI treatment is investigated and studies on how cyclic loading affects the induced beneficial compressive residual stresses are carried out. The project is executed in three different stages.

Stage 1 mainly concentrates on evaluating methods to simplify the modelling of the HFMI treatment. The goal is to reduce the computational effort without compromising the accuracy of the results. Simulations are performed on a simple cuboid geometry, also provided by the benchmark exercise, with varying parameters such as the constitutive hardening model, e.g. isotropic or kinematic or Chaboche, the analysis type, e.g dynamic or quasi-static, and the indenter tool model, e.g., a single tool or several tools applied in sequence. It is concluded that the choice of analysis type impacts the residual stress state to a minor extent, while it greatly affects the computational effort. A clear trend shows that with an increasing number of indenter parts, greater computational effort is required. Using a single indenter proved to give comparable results to previous work and a uniform residual stress profile. Since it is also computationally effective, it is concluded that this method is the most suitable.

The simplifications are then carried over into Stage 2, where the HFMI treatment is applied to the welded coupon geometry. In this stage, the indenter tool models from Stage 1 are redesigned to fit the coupon and simulations are performed to further evaluate the models. Simulations are performed with a variety of indenter tool models. The simulations with several indenters moving in sequence show a greater variation in the residual stress profile, suggesting some unreliability in this method. It is determined that a five-part single impact model was the the most suitable.

Finally, in Stage 3 the coupon model with induced residual stresses from a single impact HFMI simulation is subjected to cyclic membrane loading. The residual stress state is found to not be significantly impacted by constant amplitude loading. However, after variable amplitude loading the beneficial residual compressive stresses are found to be redistributed. Furthermore, the beneficial residual compressive stresses are removed to a greater extent when increasing the maximum applied nominal stress. When applying nominal stress with a peak load of 75 % of the yield limit, the beneficial residual compressive stresses are reduced by almost 100 %. However, when applying a nominal stress with a peak load of 63 % of the yield limit, they are only reduced by 50 %.

For simulating HFMI, the results suggest using the Chaboche mixed hardening model with quasi-static analysis using a single impact indenter tool model. For future work it is recommended to perform further investigation of the single impact dynamic simulations using kinematic hardening since it showed promising results. Furthermore, to achieve better understanding of the effects of cyclic loading, simulations with a wider range of load amplitudes, and closer investigations of the stress-strain development during loading, are recommended.

Contents

List of Figures

List of Tables

Nomenclature

Abbreviations

C3D8	8-node linear hexahedral elements
CA	Constant amplitude
FEA	Finite element analysis
HFMI	High frequency mechanical impact
ISSC	International Ship and Offshore Structures Congress
L	Longitudinal
MIS	Multiple impact simulation
R3D4	Rigid 3-D 4-node bilinear rigid quadrilateral element
SIS	Single impact simulation
T	Transverse
TT	Through-thickness
VA	Variable amplitude

Symbols

ΔS	Nominal stress range
γ_1, γ_2	Chaboche dynamic recovery parameters
λ	Load factor
μ	Friction coefficient
ν	Poisson's ratio
σ	Stress
σ_0	Initial yield in the Chaboche model
σ_{y}	Yield stress
ε_p	Plastic strain
C_1, C_2	Chaboche model kinematic hardening parameters
E	Elastic modulus
k_{t}	Stress concentration factor
R	Ratio between minimum and maximum applied load in VA loading
S_{min}	Minimum nominal stress
S_{max}	Maximum nominal stress

Indenter model naming convention

A	Angled indenter
mir	Mirrored indentation pattern
MSIS	Multiple single impact simulation
seq	Sequential indentation pattern
SIS	Single impact simulation
XP	X number of parts

1 Introduction

The numerical simulation of complex objects such as ships and complex processes such as welding is often used to replace or supplement costly full-scale experiments. Even so, numerical simulation, e.g. finite element analysis (FEA), can itself be comparatively computationally demanding and costly. Consider, for example, fully three-dimensional (3D) FEA of welding followed by different post-weld treatments and then by cyclic loading. Simplified models can be effective when making comparisons between different approaches in this complex three-part process. [1]

The process of simulating High Frequency Mechanical Impact (HFMI) treatment, a form of peening [2], of welds is computationally costly and knowledge of how well the beneficial effects of HFMI remain after cyclic loading is desirable. To further study HFMI, a benchmark exercise has been created in the Specialist Committee V.3 Materials and Fabrication Technology of the International Ship and Offshore Structures Congress (ISSC 2018) [3]. The benchmark exercise aims to develop design guidelines for the use of HFMI treatment in welded structures in the ship building industry.

1.1 Background

Welding is a fabrication process for joining materials, usually metals or thermoplastics, by the application of heat. It has had a significant impact on a large number of industries, including the ship building industry, where it has replaced the less productive method of riveting.

The high heat production in the welding process gives rise to large thermal gradients, which create physical and metallurgical changes in the welded specimen. During cooling the weld material thermally contracts locally, which yields the material and creates tensile residual stresses in the weld material, which make it more prone to failure. The geometry at the weld toe also induces stress concentrations, which further reduce the fatigue life of the welded metal and increase the risk of crack initiation [4]. Several methods exist for reducing these adverse effects. These include post-weld stress relief, the use of low temperature transformation electrodes, or HFMI.

In HFMI, the weld area is subjected to repeated impacts by a cylindrical pin with a rounded tip (indenter), with a radius of 2 mm, at a frequency of approximately 100 Hz, moving with a velocity of approximately 12 cm/min along the weld. The pin indents roughly 0.2 mm into the material, in the direction of the tool. HFMI is one of the most recent post-weld treatment methods which is used to increase the fatigue life of welded components [4]. The increase in fatigue life from HFMI is due to the combination of the change in geometry and the introduction of compressive residual stresses at the weld toe.

A specific coupon geometry, with a high stress concentration at the weld toe, is used for the benchmark exercise [3]. The geometry, as shown in Figure 1, is a stiffener, fillet welded to a plate which is subjected to cyclic membrane loading. The current project, for TME131, will contribute to Chalmers University of Technology's submission to the benchmark exercise. The main aspect of the project is to, with use of FEA, study to what extent the beneficial effects of HFMI remain after application of cyclic constant amplitude (CA) loading and cyclic variable amplitude (VA) loading. In doing so, thereby contribute to the development of design guidelines for the use of HFMI treatment.

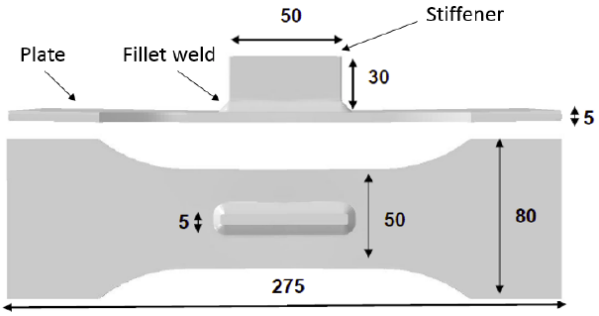

Figure 1: Coupon geometry [mm] [1]

1.2 Project goal

The overarching goal of the project is to contribute to the ISSC 2018 benchmark on HFMI. This is done by documenting the effects of cyclic membrane loading on the residual compressive stresses that HFMI treatment has induced in the coupon. A subgoal is to obtain an indentation simulation process that gives rise to a residual stress field comparable to those found in previous experiments and simulations, e.g. [3], without excessive use of computational power.

1.3 Project approach

The project aims to fulfil the project goals through three stages of FEA. In the first two stages, the HFMI treatment will be modelled as a simplified process where an indenter tool is pushed down once or a few times, instead of simulating the thousands of impacts that actually occur during HFMI treatment. In the third stage, cyclic membrane CA and VA loading will be applied to the coupon.

In Stage 1, simulations of different indenter tool models, e.g. single impact or multiple impact, hardening models, e.g. kinematic or isotropic or Chaboche, and analysis types, e.g. quasi-static or dynamic, will be performed on a simplified cuboid model. The residual stresses through the thickness will be evaluated in longitudinal and transverse directions to compare to previous experiments and simulations, e.g. [3], to find a suitable indentation simulation process. In Stage 2, these results will be adapted to the coupon model to evaluate the residual stresses at the weld toe along two specified paths to compare to previous experiments and tests, e.g. [1]. In Stage 3 the coupon model will be subjected to CA and VA loading to study the effects of cyclic membrane loading on the residual compressive stresses that HFMI has induced in the coupon. The results will be compared to previous research, e.g. [5].

2 Finite element models

Fully meshed models for the cuboid and coupon have been developed and provided by the benchmark exercise and are used by all participants, including the current project. The material specified in the models is S355, a structural steel with a minimum yield limit of 355 MPa. The material has a Young's modulus of 202 GPa, Poisson's ratio of 0.3 , and density of 7.9 kg/m^3. As mentioned in Section 1.2, a fine meshed test cuboid was used to test variants of simulating HFMI.

2.1 Test cuboid

A simple cuboid shaped test specimen was used to investigate the residual stress field after application of HFMI with varying analysis types, hardening models and indenter tool models. The model was 10x10x20 mm^3 meshed with 105000 linear hexahedral elements (C3D8) with a refinement along the penning path, as shown in Figure 2. The smallest elements were 0.2x0.2x0.2 mm^3. Since the peening process is symmetrical in the transverse direction (T), one face of the cuboid was specified as symmetrical by a boundary condition and the peening was done on this edge. The length of the peening path was 10 mm placed at the centre of the cuboid longitudinally (L). Stresses were analysed along a path going through the thickness (TT), starting from the centre of the peening path.

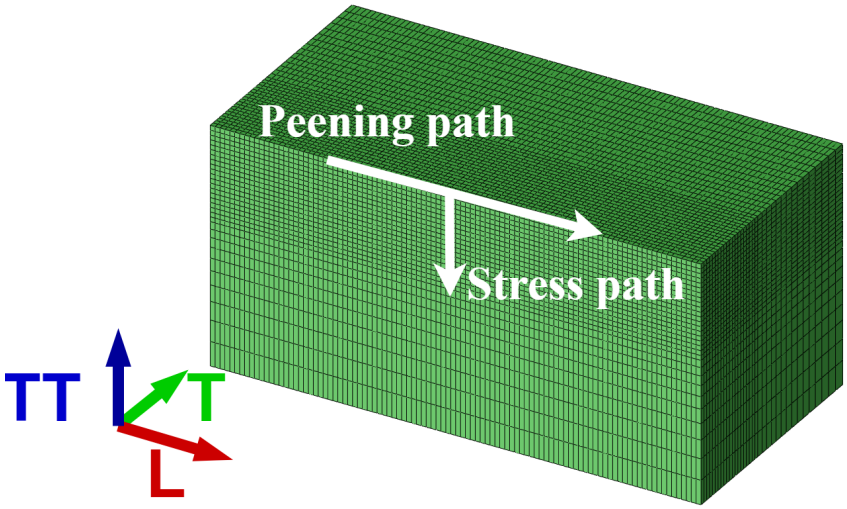

Figure 2: Cuboid model and paths

2.2 Coupon model

The used coupon model was a stiffener, fillet welded to a plate, as shown in Figure 3a. The coupon was symmetric in the longitudinal direction, and therefore only half of the coupon was analysed. The model was stress free before the HFMI process, i.e., no residual stresses caused by the heat from the welding process were taken into account. Furthermore, the used material was homogeneous. The used mesh consisted of 37552 linear hexahedral elements (C3D8) with a refinement around the weld toe to capture the stress gradients due to HFMI and the cyclic membrane loading. Stresses were examined along Path A and B, as shown in Figure 3b. For cyclic loading stresses were also examined in the node where Path A and B originate, further noted as the weld toe node.

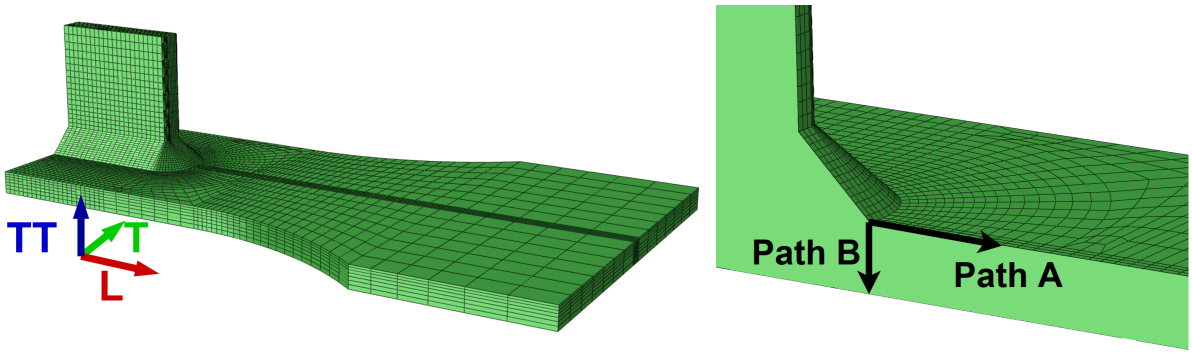

(a) Coupon model

(b) Coupon paths

Figure 3: Coupon model and paths

After inspection of the supplied coupon mesh it was discovered that it contained some duplicate elements, shown in green in Figure 4a. Furthermore, it was found that the weld region of the coupon geometry contained unconnected nodes in some elements, shown in blue in Figure 4a. The unconnected nodes are further illustrated in Figure 4b where it is clear that the nodes of the blue elements are not connected to the surrounding red elements.

Rectifying the model reduced the total number of elements by 392, from 37552 to 37160. The unconnected nodes were located on only one side of the weld toe causing an asymmetry, which in turn might have caused erroneous results to some extent.[1] This issue is further analysed in Section 4.4, where it is seen that elements on Path A and B, which are critical for the purposes of comparison with previous work, were not affected to a large extent before cyclic loading was applied.

All results presented in Section 3.2.3 were obtained using the supplied coupon mesh. However, the results in Section 3.3.3 were obtained using the rectified mesh.

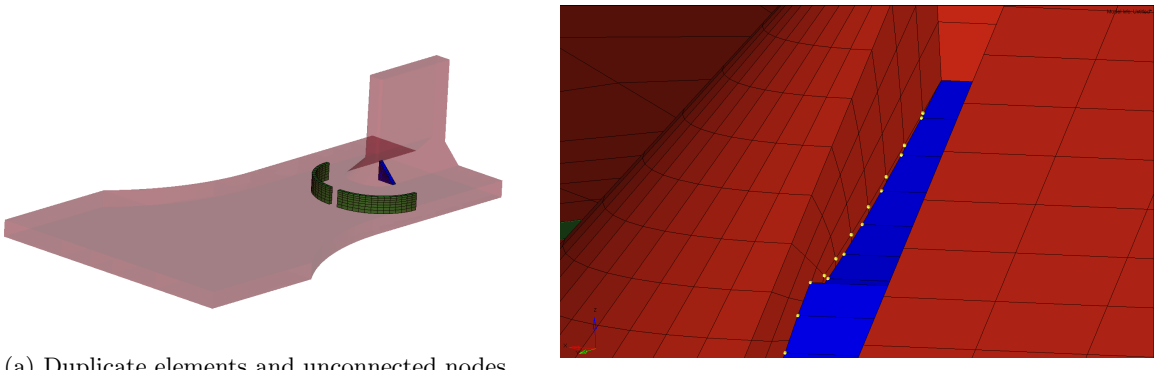

(a) Duplicate elements and unconnected nodes

(b) Unconnected nodes

Figure 4: Faults with supplied coupon mesh

[1]This information has been relayed to the other participants in the benchmark exercise and the corrected mesh is now available to them.

3 Finite Element Analysis

In HFMI, an indenter tool impacts the subjected specimen with sufficient kinetic energy to create plastic deformation and compressive stresses. There are many physical processes involved in this, including the tool-specimen mechanical contact, yielding inducing large deformations, subsequent hardening of the material, the inertia effects of the material that is set in motion, and heat generation. Simulation of all these processes for every impact is very computationally expensive, and therefore it is desirable to make significant simplifications of the process, while retaining accuracy in the results.

In previous research, e.g. [1], a number of different simplifications have been used. These include having an indenter tool that is extended along the weld, which leads to every impact indenting a larger part of the weld, so that the number of impacts can be significantly reduced. Furthermore, different hardening models have been used, and the problem has been modelled as both dynamic and quasi-static. The results with simplified modelling have been compared to experimental studies [5] and advanced, computationally expensive finite element analysis [6].

For the purposes of this project, it was assumed that the heat generation during HFMI treatment is negligible. The HFMI simulations will also be conducted on a stress free, materially homogeneous model, which means that residual stresses and metallurgical variations created by welding are not accounted for.

The FE simulations were divided into three stages: Stage 1: Simplified HFMI evaluation using the cuboid, Stage 2: HFMI treatment of the coupon, and Stage 3: Cyclic membrane loading of the coupon. The purpose of Stage 1 was to conclude which simplifications of the HFMI process could be suitable in practical use. These simplifications were then implemented and results compared in the HFMI treatment simulation of the coupon in Stage 2. Lastly, the coupon with applied HFMI would be used in Stage 3, where the goal was to see how well the coupon retained the beneficial stresses created in Stage 2 when subjected to different types of cyclic loading, with both CA and VA loading.

These simulations were run on Chalmers computers and resources at Chalmers Centre for Computational Science and Engineering (C3SE) [7] provided by the Swedish National Infrastructure for Computing (SNIC). All simulations were carried out using ABAQUS v.6.14 [8].

3.1 Stage 1: Simplified HFMI evaluation using the cuboid model

The first stage of the FEA investigated how to model HFMI treatment with as low computational effort as possible while maintaining comparable results to physical experiments and other simulations [3, 6], performed on the cuboid model as shown in Figure 2. The aim was to recommend simulation procedures for Stage 2 and future work in the benchmark exercise. The constitutive hardening model, the analysis type, and the indenter tool model were studied.

3.1.1 Boundary conditions

The boundary conditions previously used by participants in the benchmark exercise were applied [3]. Specifically, to account for the symmetry along the peening path, displacements were restricted in the transverse direction as were the rotations around the longitudinal and through-thickness axes on the nodes as shown in Figure 5a. To prevent translation of the cuboid, the entire bottom surface, as shown in Figure 5b, was constrained in longitudinal, transverse, and through-thickness directions.

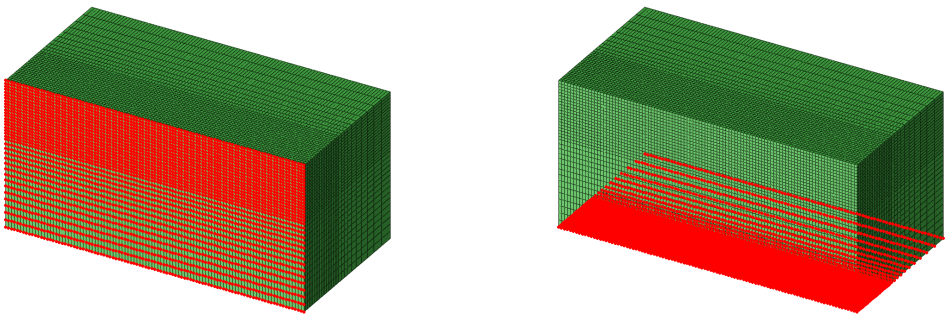

(a) Symmetry boundary condition (b) Fixed boundary condition

Figure 5: Nodes for boundary conditions on the test cuboid shown in red

3.1.2 Constitutive hardening models

As plasticity occurs when performing the HFMI treatment, a material hardening model was required. The hardening models studied were isotropic hardening, kinematic hardening, and the Chaboche mixed isotropic and kinematic hardening model. [9]

In previous work, e.g. [3], the Chaboche hardening model had been proven to give comparable results to experimental data. Table 1 shows the material parameters for the Chaboche hardening model used for the steel S355J2H.

Table 1: Chaboche material parameters [3]

σ_0 [MPa]	C_1 [MPa]	γ_1 [-]	C_2 [MPa]	γ_2 [-]
435	8971.8	218.65	12654.8	106.98

The isotropic and kinematic hardening model parameters were based on a tensile stress test performed on a specimen of S355J2H [10], in which true stress and plastic strain were measured in the specimen, as shown in Table 2.

Table 2: Plastic strain - stress response [10]

Material parameter	Data points								
ε_p [-]	0	0.005	0.01	0.03	0.05	0.1	0.3	0.5	0.8
σ [MPa]	390	464	478	536	581	620	660	670	700

For both the kinematic and isotropic models it was decided to use a linear hardening model, as ABAQUS limits the kinematic hardening model to a linear one. As such only two values were required, one of which had to be the yield stress at zero plastic strain. Several pairs of values in Table 2 were tested with kinematic and isotropic hardening to ensure that similar results were obtained from one loading procedure. The test was performed on a test cuboid similar to the one described in Section 2.1 but with a coarser mesh, to be able to run quick simulations. The tests were run with one single indentation and the residual stresses along a path through the thickness in the middle of the peening path were extracted. As there is only one indentation, the Bauschinger effect [2] should not influence the results and therefore the models should behave similarly. It was noted that the residual stress state was heavily influenced by which data points were chosen, especially for the kinematic model. In previous work [1] the points $\sigma = 620\,\mathrm{MPa},\ \varepsilon_\mathrm{p} = 0.1$ was used for this comparison. Although, as shown in Figure 6a, these data points do not give very similar results for isotropic and kinematic hardening. Data points for a lesser plastic strain than $\varepsilon_\mathrm{p} = 0.1$ showed even greater divergence between the models. From the tests done on the coarse meshed cuboid it was established that $\sigma = 670\,\mathrm{MPa},\ \varepsilon_\mathrm{p} = 0.5$ yielded the most consistent results, as shown in Figure 6b.

[2] The Bauschinger effect, present in the kinematic hardening model, is the lowering of the elastic limit in compression following a tension in the plastic region during repeated cycles [11].

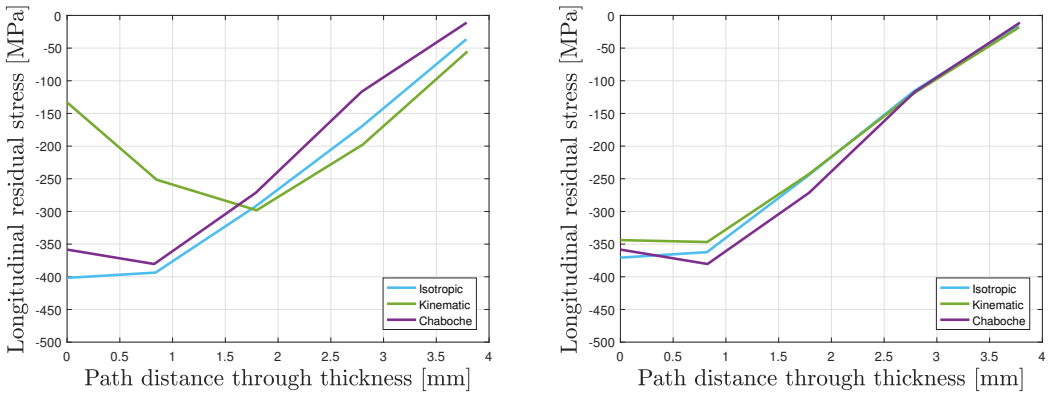

(a) $\sigma = 620\,\text{MPa},\ \varepsilon_\text{p} = 0.1$ (b) $\sigma = 670\,\text{MPa},\ \varepsilon_\text{p} = 0.5$

Figure 6: Comparison of the isotropic, kinematic and Chaboche models

3.1.3 Choice of analysis type

In the work summarised by the ISSC 2018 [3], three analysis methods have been used with varying results. In the current study it was noted that further investigation was needed to recommend design guidelines for use of HFMI simulations. The three analysis types considered were quasi-static, dynamic implicit, and dynamic explicit.

The quasi-static analysis is a time-independent analysis, which means that no consideration is taken to the dynamic effects and therefore it neglects both inertia terms and time-dependent material effects [9]. A static general step was set up in ABAQUS for both loading and unloading. The total step time, initial increment, and minimum and maximum increment sizes were then set, allowing for convergence to be achieved. The following values were used throughout the quasi-static analyses [9]: total step time = 1 s, initial increment = 0.5 s, minimum increment size = 1E-5 s and maximum increment size = 0.5 s.

Dynamic implicit and dynamic explicit are time-dependent analyses since dynamic effects are taken into account. Therefore, it is important to set the proper time period for the procedure. What differs between the two is how the problem is solved. Specifically the implicit analysis, just like the quasi-static analysis, solves the problem in an iterative manner. However, the explicit analysis uses a central-difference integration method, solving for the accelerations. In general, the explicit analysis is very efficient at solving problems with short dynamic response times [9].

Both dynamic analyses used a time period of 0.05 s during loading, with a short resting period after to account for any dynamic effects still taking place. This time period was implemented when issues arose while trying to simulate with the proper procedure time 0.0005 s, corresponding to 100 Hz. Excessive distortions occurred in some elements, causing the simulations to fail. As time did not allow for this issue to be investigated and corrected, the longer time period was used.

3.1.4 Indenter tool models

In an attempt by [2] to simplify the simulation of the HFMI process, the Multiple Impact Simulation (MIS) of the indenter tool was assumed to be replaceable by one single indentation along the entire peening path. Simulations were performed with good results of the longitudinal stresses in the through-thickness direction [3], while the transverse stresses diverged somewhat from previous experimental and simulated results. In the simplified process this technique was simulated as shown in Figure 7a, from now on noted as Single Impact Simulation (SIS).

To better emulate MIS, the tool from SIS was divided into four parts. These parts were pressed down into the cuboid, one at a time, sequentially along the peening path, as shown in Figure 7b. This technique is further denoted as Multiple Single Impact Simulation (MSIS). To analyse the importance of the order of impact in MSIS, further simulations were also performed in a mirrored sequence, as shown in Figure 7c.

The indentation depth was predefined to 0.2 mm into the cuboid [3]. Therefore, the tool was displacement driven and no particular load was specified. The indentation procedure also depended on which analysis

type was used, where the dynamic simulations required a set indentation time and loading curve, which the quasi-static analysis did not. This loading curve was defined as half a negative sine wave with a period time of 0.1 s and an amplitude of 0.6 mm with the indenter starting 0.4 mm above the surface.

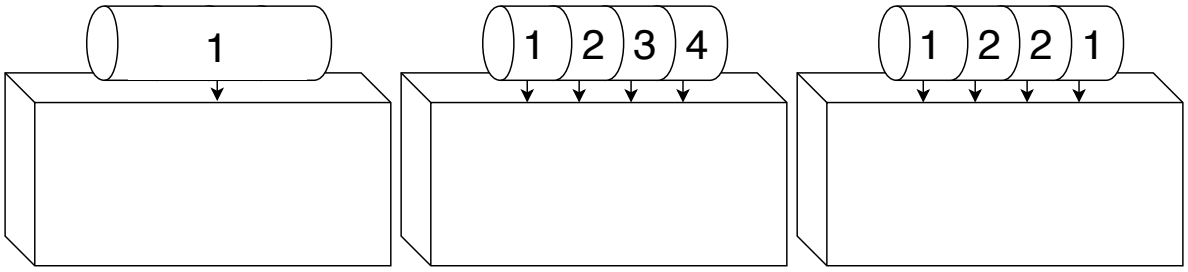

(a) SIS (b) MSIS-seq (c) MSIS-mir

Figure 7: Impact order for HFMI simulations. Order illustrated by number inside the indenter

3.1.5 Contact model

For all HFMI simulations, mechanical contact properties were defined for the interaction between the indenter and the cuboid model. The interaction was set as a surface to surface condition with the indenter as the master and the cuboid as the slave. The tangential interaction was set as a friction penalty, with simulations being conducted with a friction coefficient of $\mu = 0.15$ or $\mu = 0.3$, as used by [3]. The normal interaction was set as a hard contact using the standard ABAQUS definition. No interactions were defined between separate indenter parts or between the cuboid and the side of the indenter. To facilitate convergence a small overlap was introduced between indenter tools.

3.1.6 Results and conclusions from Stage 1

Stage 1 of the project aimed to investigate three different hardening models, three analysis types, and three indenter tool models, resulting in a total of 27 simulations. The main priority, due to the short time span of the project, was to run all nine simulations for SIS. This is the simplest indenter tool, which made it desirable to find a hardening model and a simulation type that gave comparable results to physical experiments.

Initially the friction coefficient was changed between $\mu = 0.3$ and $\mu = 0.15$. Since the results were very similar and the latter was used by a majority of the participants in [3], that value was used for the results presented in Figure 8. Figures 8a and 8b show only SIS with a comparison of different hardening models and simulation types as was the focus of Stage 1. For comparison, the experimental data from ISSC 2018 [3] and Foehrenbach [6] have been used. The best SIS results are then compared to the MSIS results with quasi-static analysis and the Chaboche hardening model in Figures 8c and 8d.

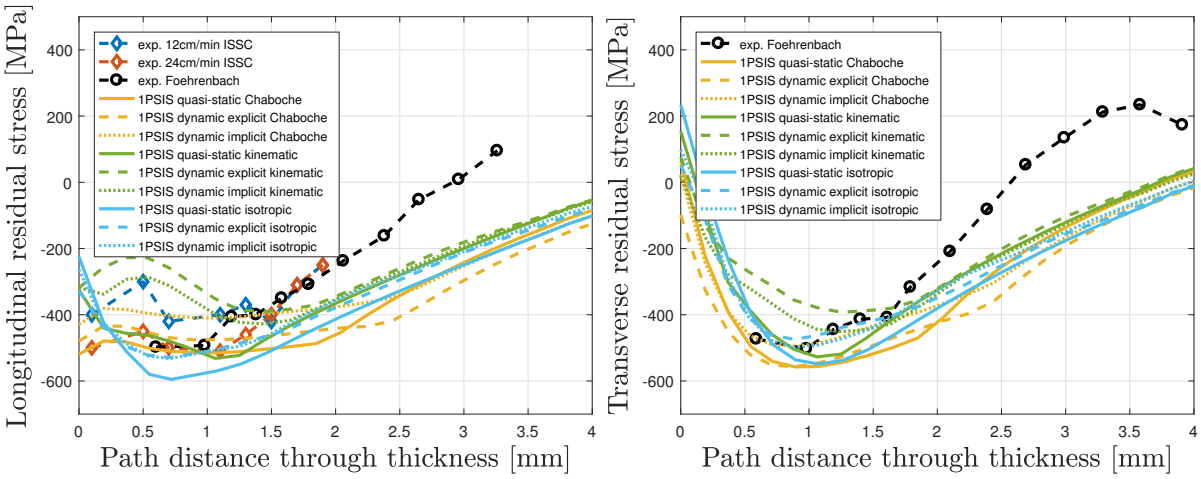

(a) SIS comparisons with different hardening models and analysis types

(b) SIS comparisons with different hardening models and analysis types

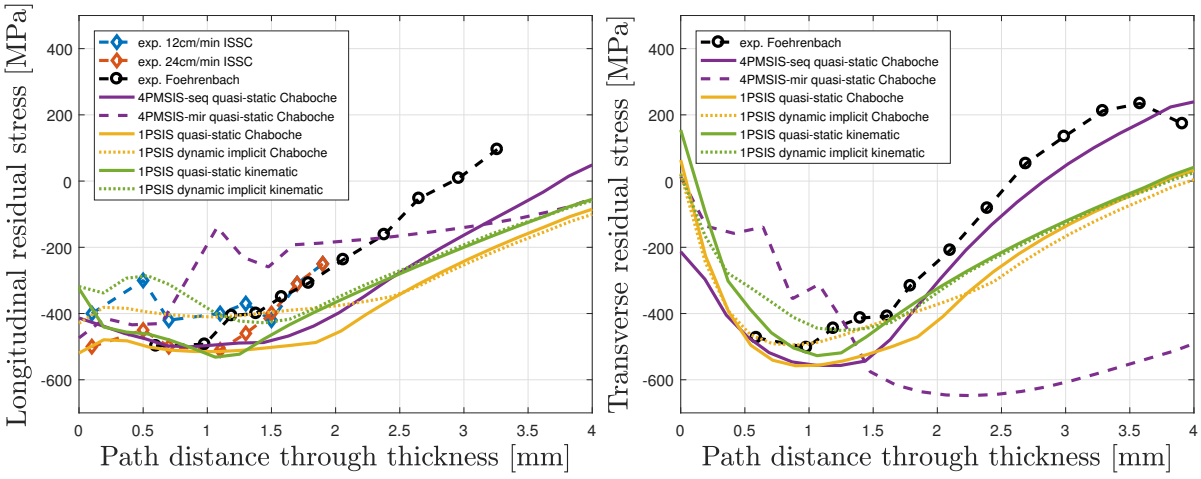

(c) MSIS against best SIS

(d) MSIS against best SIS

Figure 8: Stress comparison of different simulation variations vs ISSC 2018 [3], Foehrenbach [6]

For the longitudinal stresses using SIS, Figure 8a, the quasi-static simulation with kinematic hardening followed the experimental results from Foehrenbach and 24 cm/min ISSC 2018 best in the first 1.5 mm. Transverse stresses for SIS followed a strict trend regardless of simulation type and hardening model, as seen in Figure 8b. However, most simulations resulted in greater compressive residual stresses when compared to experimental data, especially from 2 mm to 4 mm depth.

With MSIS, the result varied to a greater extent, giving both better and poorer conformity with what has been found in earlier research [3, 6]. The mirrored quasi-static simulation with Chaboche hardening gave poor results for both longitudinal and transverse residual stresses when compared to the physical experiments. This is thought to be because the two outer indenters displaced material towards the centre of the cuboid and hardened it, creating unpredictable material behaviour. On the other hand, MSIS-seq quasi-static with Chaboche hardening gave the best results of all simulations both longitudinally and transverse, as shown in Figures 8c and 8d. However, further investigation showed that the residual stress state was heavily dependent on the location from where data were extracted in the longitudinal direction on the peening path, as seen in Figure 9. As each indentation occurred the stress state from previous indentation was shifted along the path. The same effects are likely seen in real world application of the HFMI treatment. However, in practice the steps taken are much smaller, creating a more uniform residual stress profile. For this reason, it can be argued that SIS simulation may give more realistic results, as it creates a uniform residual stress profile.

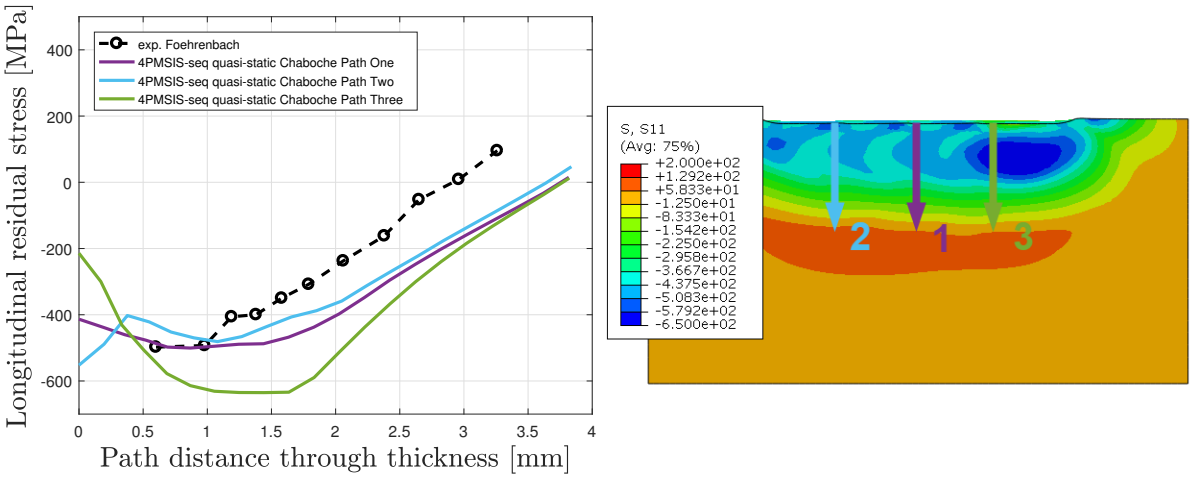

(a) Longitudinal residual stress comparison of three paths using MSIS-seq

(b) Three stress paths on the cuboid model's symmetry plane

Figure 9: Path comparison vs. Foehrenbach [6]

To evaluate the computational effort of different simulations, the total CPU times were compared, as shown in Table 3. The 1PSIS dynamic explicit had the lowest computational effort, making it the most desirable analysis type in this regard. It was also noted that the constitutive hardening model had negligible effect on the computational effort, and hence different hardening models were not included in Table 3. The total step time in the quasi-static simulations was different, as every load step was simulated with a duration of 1 s, possibly causing a discrepancy in the comparison. However, with a smaller total step time, a lower time increment would be needed for convergence which possibly invalidates this concern.

Table 3: Comparison of computational effort and results

Simulation	Total CPU time [s]	Number of load steps
1PSIS quasi-static	11438	2
1PSIS dynamic explicit	5694	1
1PSIS dynamic implicit	25120	1
4PMSIS-mir quasi-static	99678	3
4PMSIS-seq quasi-static	44333	5

From the results in Stage 1, recommendations could be made for continuing work in Stage 2. It was concluded that SIS quasi-static with Chaboche hardening model was to be implemented. Since the results from MSIS were interesting, further investigation of this approach was recommended for Stage 2 and future research. The tangential friction coefficient for the mechanical contact was set to $\mu = 0.15$, but all other contacts were defined as mentioned in Section 3.1.5 for Stage 2.

3.2 Stage 2: HFMI treatment of coupon

The aim of Stage 2 was to create the beneficial compressive residual stresses with as similar stress field as possible to that of physical HFMI. The main contribution to the benchmark was to study the remnants of these stresses after cyclic CA and VA loading. In Stage 2 the indenter tool geometry were adapted to fit the coupon model with recommendations from Stage 1 considered to get as physically realistic stresses as possible.

Several simulations of HFMI treatment were performed on the coupon geometry. Indenter tool models were created and analysed based on longitudinal and transverse residual stresses along Paths A and B. Based on the conclusions from Stage 1 in Section 3.1.6, the Chaboche mixed hardening model and quasi-static analyses were used for all HFMI simulations in Stage 2

3.2.1 Boundary conditions

For the simulation of the HFMI treatment, the lower surface of the coupon was fixed in the through-thickness (TT) direction, as shown in Figure 10a. This was done to mimic the effect of the coupon lying on a flat table. In-plane movements were still allowed for this surface, which means that friction effects at the table-coupon interface were neglected. This boundary condition also prevents rigid body motion in the through-thickness direction, and rigid body rotation around the longitudinal (L) and transverse (T) axes. Furthermore, all nodes on the end symmetry plane were constrained with a symmetry condition in the longitudinal direction, as shown in Figure 10b. This prevents rigid body translation in the longitudinal direction and rotations around the through-thickness and transverse axes. Additionally, to prevent rigid body motions in the transverse direction all nodes along the longitudinal sides of the coupon were fixed in the transverse direction, as shown in Figure 10c. Originally, only one node on the symmetry plane was fixed in the transverse direction. However, as simulations were conducted where the indentation sequence was not symmetrical in the transverse direction this node was loaded excessively, requiring a change of the boundary condition.

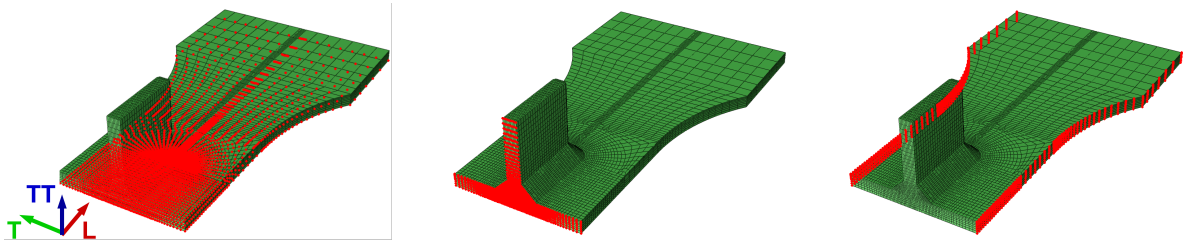

(a) TT boundary condition (b) Symmetry boundary condition (c) T boundary condition

Figure 10: Nodes for boundary conditions for HFMI simulations shown in red

3.2.2 Indenter tool models

The tool cross section was modelled in CATIA V5 [12] as a rectangular shape with one circular side, as shown in Figure 11c. The models were imported into ABAQUS as discrete rigid bodies and the surface meshed with 3D 4-node rigid bilinear quadilateral elements (R3D4) with an approximate element length of 0.5 mm. This element size matches the smallest element size in the contact area of the coupon model. Indenter tools with and without an impact angle of 75° were simulated to analyse the effect of the impact angle. To have comparable results, both the angled and straight indenter were positioned such that during the initial impact the tool was in contact with both weld and plate, as shown in Figures 11a and 11b.

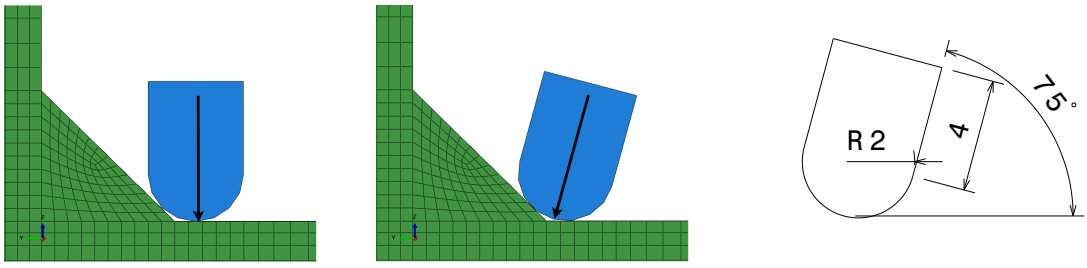

(a) Impact of straight indenter (b) Impact of angled indenter (c) Indenter cross section

Figure 11: Impact and geometry of indenter. Indentation path illustrated by black arrow

Several indenter tool designs and indentation patterns were simulated. To analyse the importance of indenting the area around the weld toe node with a single, part both four- and five-part indenter tool designs were created, as shown in Figure 12. The five-part design had an additional part that indented the area around the weld toe node. For the four-part design, that area was indented by the part that also indented the corners.

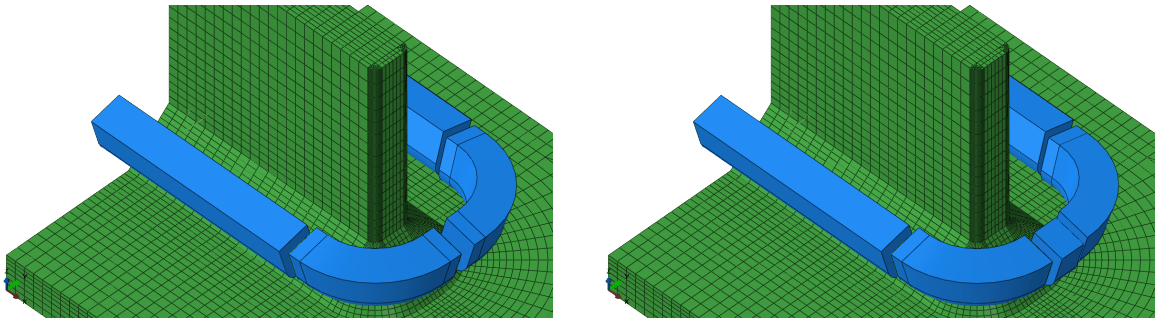

(a) Four-part indenter design

(b) Five-part indenter design

Figure 12: Indenter tool designs

Displacements were prescribed in the axial direction of the tool resulting in an indentation depth of 0.2 mm into the coupon along the weld. All other degrees of freedom were fixed. For the indenter tool with an impact angle, the boundary conditions for the corner were prescribed in a plane 45° offset from the L-TT plane around the TT axis. This resulted in only the centre of the curve impacting perpendicular to the weld.

3.2.3 Results and conclusions from Stage 2

The longitudinal residual stresses in Figures 13a and 13b are compared to data from [1]. It can be observed for both Path A and B, previously described in Figure 2.2, that no indenter tool model follows the data particularly well, but most tools are in the same vicinity. Furthermore, it should be noted that the data from [1] were gathered by taking the data from "conventional weld + HFMI" and reducing it by the data for "conventional as-welded", i.e., it is stress the redistribution caused only by HFMI that is compared.

As can be seen in Figure 13, 5PAMSIS-seq displayed some unexpected results. For example, in Path B the longitudinal residual stresses are tensile, which should not occur. On the contrary, the transverse residual stresses are the most compressive achieved. Unfortunately, time did not permit study of this.

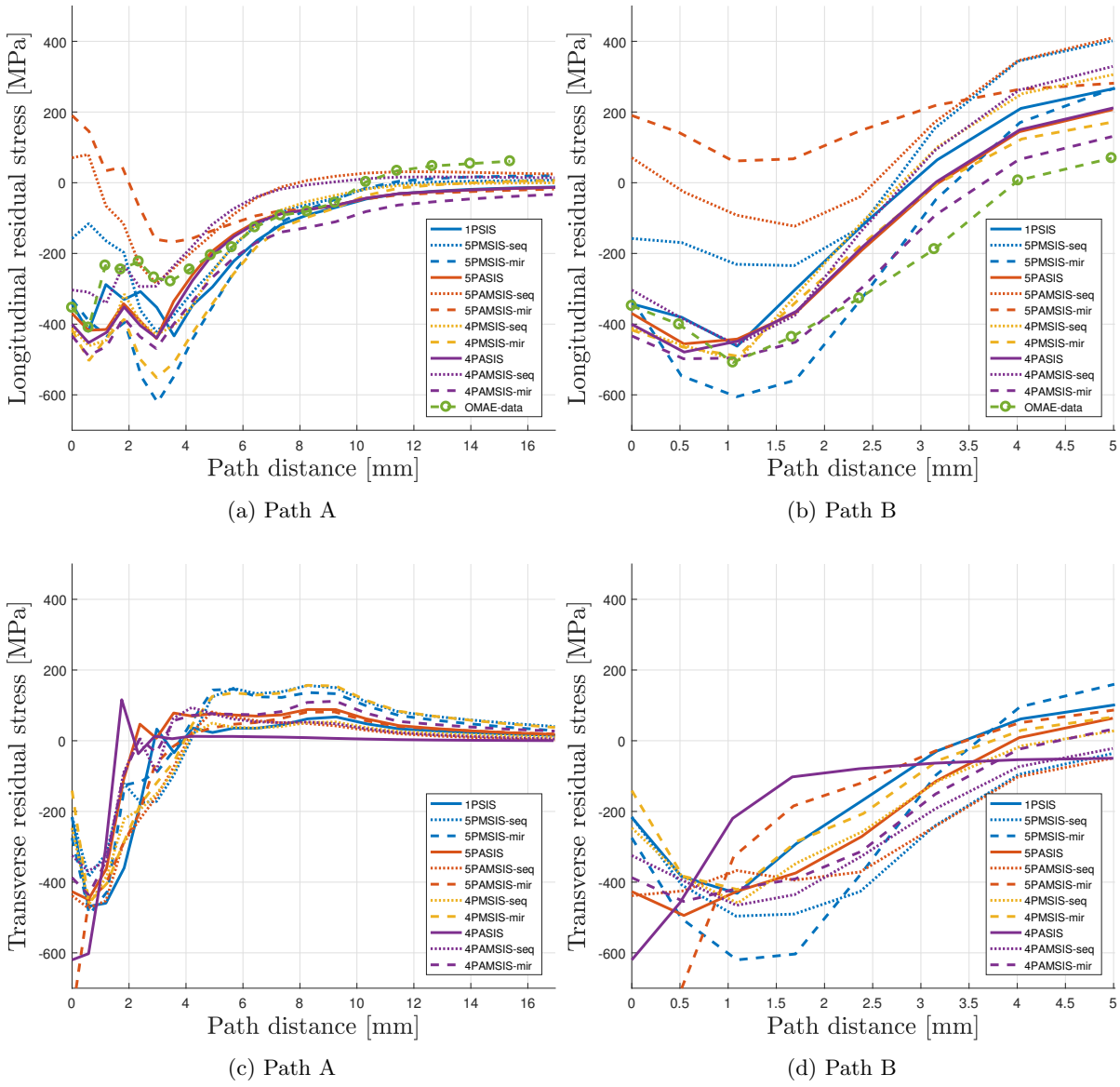

(a) Path A

(b) Path B

(c) Path A

(d) Path B

Figure 13: Longitudinal and transverse stresses for a variety of indenter tool models vs. OMAE [1]

From the longitudinal residual stress field after 1PSIS and 4PAMSIS-seq, as shown in Figure 14, several observations were made. The compressive residual stresses were primarily located in the vicinity around the weld, as is expected and preferred. Furthermore, a result of the asymmetry of the mesh mentioned in Section 2.2 can be observed on the right side in the corner of the weld in Figure 14a. These stresses were not present at the corresponding location on the left side. Additionally, an unwanted result of the asymmetrical indentation pattern for 4PAMSIS-seq is observed in Figure 14b and 15b. The residual stresses were not uniform in the transverse direction at the weld toe, nor is the magnitude of the compressive residual stresses the same for the left and right side.

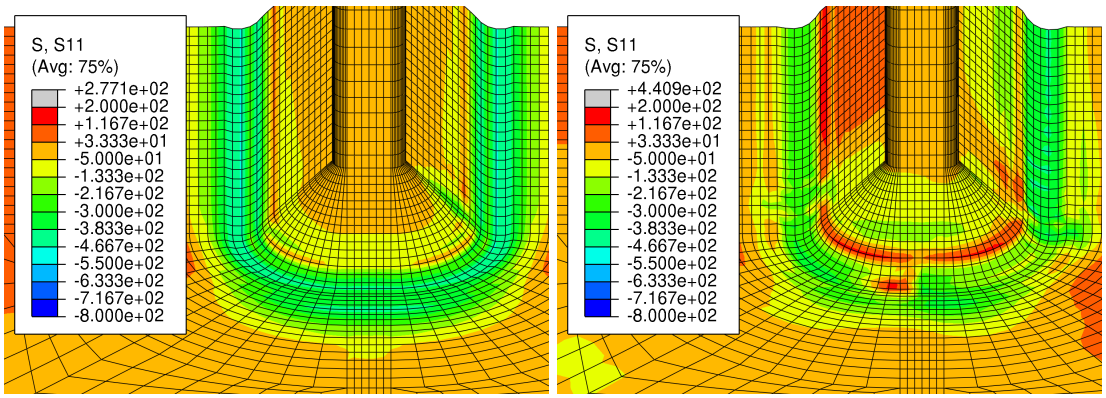

(a) 1PSIS (b) 4PAMSIS-seq

Figure 14: Longitudinal residual stresses [MPa]

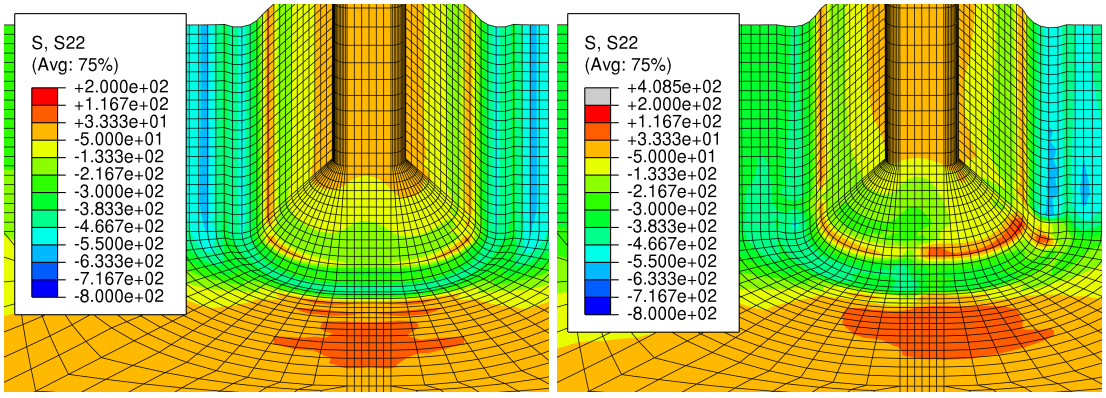

(a) 1PSIS (b) 4PAMSIS-seq

Figure 15: Transverse residual stresses [MPa]

As can be seen in Figure 16, there was a large difference in the residual deformation between 1PSIS and 4PAMSIS-seq. Furthermore, there was a large difference between the left side (L) and the right side (R) for 4PAMSIS-seq. This highlights the main issue with sequential indentation patterns; the asymmetric residual deformation and difference in the stress between the left and right sides. By comparison, the residual deformations for 1PSIS were very symmetric.

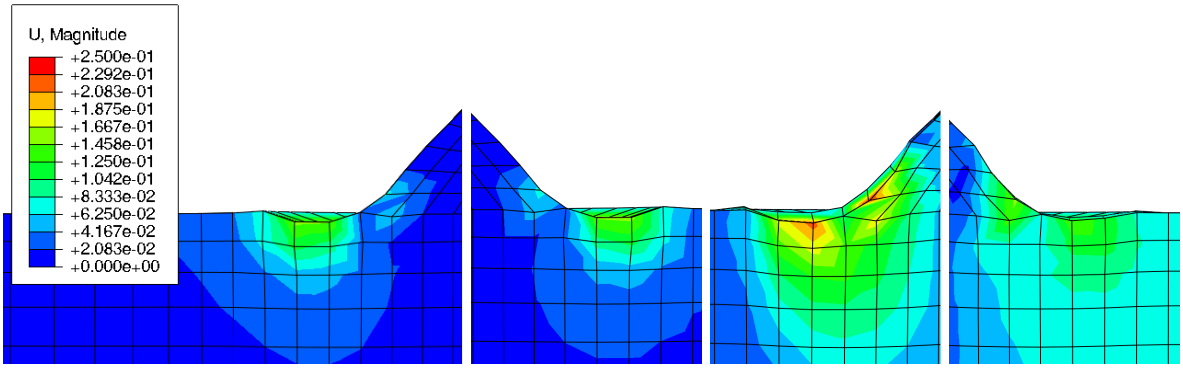

(a) 1PSIS R (b) 1PSIS L (c) 4PAMSIS-seq R (d) 4PAMSIS-seq L

Figure 16: Magnitude of deformation [mm]

A comparison of simulation times between SIS, MSIS-seq, and MSIS-mir for a four-part angled indenter

is shown in Table 4. The simulations were performed with identical minimum, maximum, and initial increment step as well as load step time. The total simulation time is approximately linearly dependent on the number of load steps.

Table 4: Comparison of computational effort for four-part analyses

Simulation	Total CPU time [s]	Number of load steps
4PASIS	12611	2
4PAMSIS-mir	22112	4
4PAMSIS-seq	41998	8

Simulations involving 11 indenter tool models were performed and the residual longitudinal and transverse stresses compared. Although MSIS may have a closer resemblance to the real HFMI treatment, the residual stress response of the simulations were inconsistent and hard to predict. For example, the longitudinal residual stresses were shown to vary greatly for both mirrored and sequential indentation order combined with four or five parts along the weld. However, 4PASIS and 5PASIS were very similar for longitudinal stresses, although the results for transverse stresses were far from similar. The 5PASIS mostly followed the trend of the other curves, however the 4PASIS did not. Furthermore, the influence of the angle of the indenter for MSIS were found to be most influential for longitudinal residual stresses along Path A and B.

Based on these conclusions, 5PASIS was chosen to be implemented in Stage 3. SIS was chosen as it is less computationally demanding, as compared to MSIS. The five-part tool was chosen as it was concluded that the indentation order, or position, was very important for the residual stress field. Therefore, having a single indenter in the area around the weld toe node would be desirable. Finally, the angled indenter tool was chosen to have comparable results to, e.g., [1].

3.3 Stage 3: Cyclic membrane loading of the coupon

The goal of Stage 3 was to examine how cyclic loading affects the residual stresses induced by the simulated HFMI treatment in Stage 2. Specifically, it was desired to draw conclusions on what types of loads could be tolerated without eliminating the beneficial HFMI-induced compressive residual stresses. The purpose of this was to provide data that can be used for the specification of design guidelines for the ISSC 2018 [3].

From the presented results in Sections 3.1.6 and 3.2.3 it was decided to continue to the cyclic simulations in Stage 3 with the 5PASIS indenter using the Chaboche hardening model. The analysis of the effect of cyclic loading on the residual stresses in the coupon was performed quasi-statically, with static equilibrium being enforced in every time step, thus neglecting any inertia effects. Since the real world loads that this simulated load is supposed to emulate are slow, the effects of inertia should be negligible.

3.3.1 Boundary conditions

For the simulation of the cyclic loading, the lower surface and symmetry end plane were fixed in the same way as in Stage 2, described in Section 3.2.1. Additionally, one node on the symmetry plane was fixed in the transverse direction to avoid rigid body motions.

3.3.2 Loads

The HFMI treated coupon was subjected to cyclic membrane loading in the longitudinal direction, applied at the free end, as shown in Figures 17 and 18. The load case was inspired by [1, 5] and expanded by [13] and believed to be representative of realistic loading on parts of a ship hull during operation. Only longitudinal stresses are studied as the stresses in this direction are assumed to be much larger than the transverse stresses during the cyclic loading. Furthermore, the longitudinal stresses are critical for opening of cracks at the weld toe node.

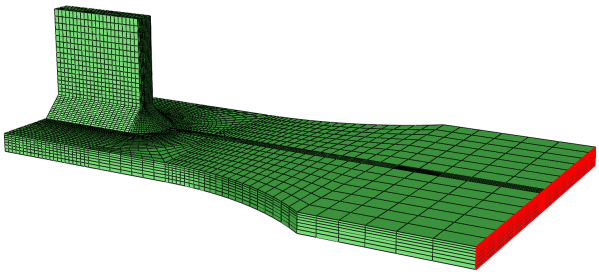

Figure 17: Surface where traction is applied shown in red

The loading was applied with a stress ratio $R = S_{\min}/S_{\max} = 0.1$, where $S_{\min}$ and $S_{\max}$ are the minimum and maximum nominal stresses respectively, as shown in Figure 18a. Simulations for CA loading were conducted for two nominal stress ranges, $\Delta S = 150\,\text{MPa}$ and $\Delta S = 250\,\text{MPa}$. The VA loading included a peak load $S_{\max}$ followed by several CA loading cycles with $\Delta S = 150\,\text{MPa}$. The loading for the peak cycles was calculated as $S_{\max} k_t = \lambda \sigma_y$. The stress concentration factor was set to $k_t = 1.6$ to account for weld toe geometry after HFMI treatment [13]. With the Chaboche material model $\sigma_y = 435\,\text{MPa}$ was used. To investigate the sensitivity in the weld toe to redistribution of the residual stresses, different $S_{\max}$ were studied by varying the load factor,λ as $0.75, 1$ and, 1.25 where $\lambda = 1$ corresponds to the stress in the stress concentration point being equal to the yield stress. To compare results with [5] a CA cyclic loading with $\Delta S = 250$ was performed.

When ABAQUS calculates the solution in a time step, the program interpolates linearly between the load input values to determine the load magnitude at that specific time step [9]. With loading as in Figure 18a, the loads will in general not be sampled at the peak values due to the time step having a finite magnitude. To ensure that the maximum and minimum loads are applied during the simulations, the load curve was manipulated to include a small plateau instead of a peak, making it possible to use a bigger time step and still capture maximum and minimum values during each load cycle. To ensure that the force was sampled at the maximum and minimum values of the modified load curves, the maximum time step during FE simulation was set to $0.399\,\text{s}$.

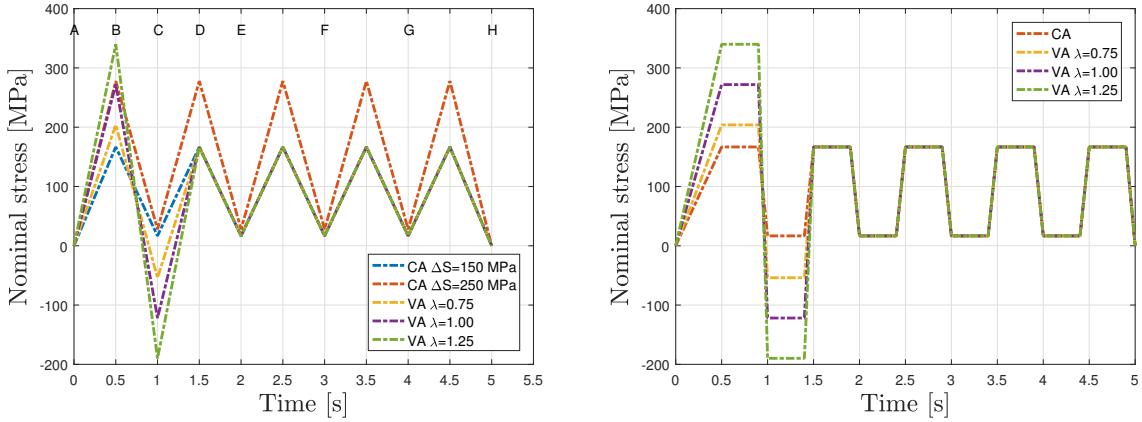

(a) Selected load cases and sampling points A-H

(b) Load curve used in ABAQUS to mitigate sampling errors

Figure 18: Desired load cases vs. definition in ABAQUS

3.3.3 Results and conclusions from Stage 3

Figure 19a shows the effect of cyclic loading on the redistribution of residual longitudinal stresses at the weld toe node for five separate load cases. Data points correspond to the loading cycles as shown in Figure 18a with data point B and D showing the stress during maximum loading, data point H showing the residual stress, and the rest of the data points showing the stress during minimum loading.

In Figure 19b the longitudinal stress vs. strain curve shows the stress-strain behaviour during VA loading

with $\lambda = 1.25$. It is noteworthy that yielding and hardening occurs not only during the peak load but also during the second load cycle. The rest of the load cycles only induce elastic deformation, as expected, cf. [5], where only the first loading cycle reduced the compressive residual stresses.

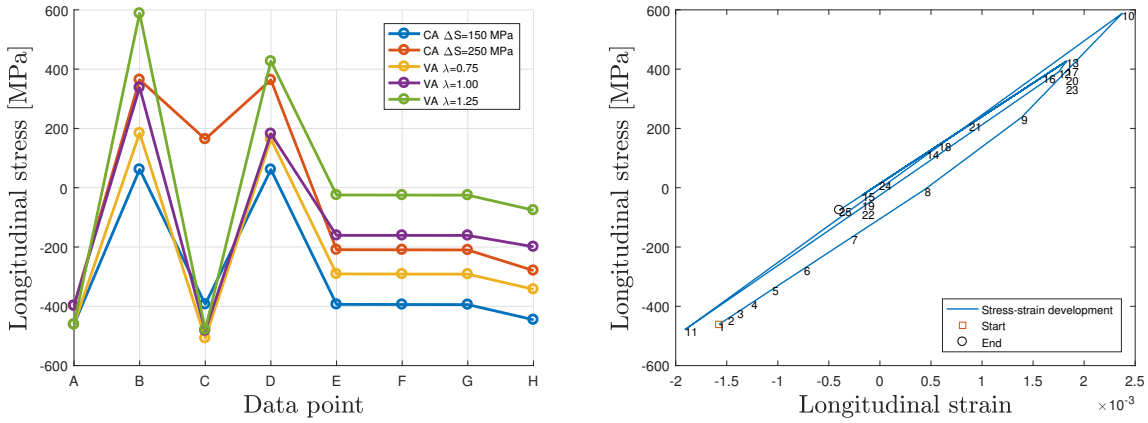

(a) The longitudinal stress, sampled at several time points during the cyclic loading. The labels on the horizontal axis correspond to the labelled time points in Figure 18a

(b) Cyclic stress-strain characteristics for VA loading with $\lambda = 1.25$. The points are sequentially labelled with numbers

Figure 19: Data in the weld toe node

Figures 20a and 20b show the longitudinal residual stresses along Paths A and B for different load cases. The value at the nodes is an average of the nearby Gauss points. The CA loading with $\Delta S = 150\,\text{MPa}$ barely redistributed any of the beneficial compressive residual stresses that were created during the HFMI treatment, which corresponds to the result shown in the last data point of Figure 19a. CA loading with $\Delta S = 250\,\text{MPa}$ reduced some of the residual stresses. The compressive residual stresses along Path A and B were almost, but not quite, eliminated during VA loading with $\lambda = 1.25$. For VA loading with $\lambda \leq 1$ the compressive residual stresses decreased in magnitude but were still present. For all loading cases at Path A, Figure 20a, the shape of the residual stress curves are similar, corresponding well with results in [1]. Contrary to [1], the shape of the curves changes along Path B, Figure 20b, for the load case VA loading with $\lambda = 1.25$. This indicates a possible change in behaviour when the peak loading exceeds VA loading with $\lambda = 1$.

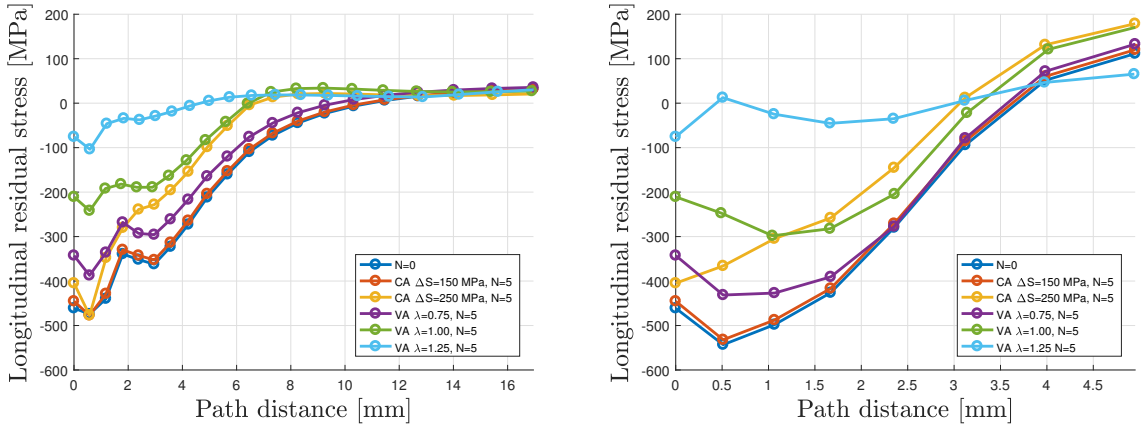

(a) Path A

(b) Path B

Figure 20: Residual stresses for varying load cases after $N = 0$ and $N = 5$ cycles

In Figure 21 the residual stress from CA loading simulations with $\Delta S = 250\,\text{MPa}$ along Path A was compared to experimental data from [5]. The experimental data is from a welded specimen, including

the heat effect of welding, while the simulated data disregard this effect. The residual stress shown for CA loading after $N = 1$, where N is the number of cycles, is estimated by reduction of the stress data from Figure 19 with the computed stress concentration $S_{\min} k_t$.

The figure shows that the main reduction of residual stress occurs during the first step, with the experimental and simulation data showing the same trend. The experimental data shows a reduction of the beneficial residual stresses with a magnitude of about 150 MPa after five load cycles. This corresponds fairly well with the simulated results, where the overall magnitude of the reduction is approximately 100 MPa. A notable difference is that the stress redistribution effect due to HFMI diminishes more quickly when moving away from the origin in the experiments than in the simulations.

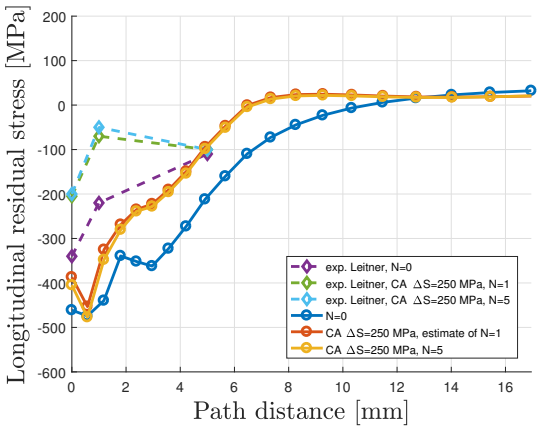

Figure 21: Experimental data from Leitner [5] compared to simulation of CA loading with $\Delta S = 250$ MPa along Path A.

When extracting the data for nodes, ABAQUS calculates an average from nearby Gauss points. Around the weld toe node there are Gauss points that are located in the weld itself. In the weld, the stress magnitude will be lower than in the plate during cyclic loading. One concern arising from this is the stress value in the weld toe node having a lower magnitude than the physically realistic value. Mainly in Path A this is a concern due to some irregularities in the data. Due to time constraints no further investigation was performed.

The impact on the beneficial compressive residual stresses due to different load cases are presented in Table 5.

Table 5: Load case impact on beneficial residual stresses after HFMI treatment

Load case	Curve effect of Figure 20a, 20b compared to $N = 0$	Reduction of residual stress
CA $\Delta S = 150$ MPa	No change	None
CA $\Delta S = 250$ MPa	Insignificant	Some
VA $\lambda = 0.75$	Same shape, shifting maximum 150 MPa	Some
VA $\lambda = 1$	Some shape change, shifting maximum 250 MPa	Halved
VA $\lambda = 1.25$	Shape change, shifting maximum 550 MPa	Complete

The longitudinal residual stress after HFMI treatment remained unchanged after CA loading with $\Delta S = 150$ MPa, suggesting that this load range is too low to induce any redistribution of the compressive residual stresses. For CA with $\Delta S = 250$ MPa the compressive stresses were reduced. Furthermore, the effects of HFMI treatment were also reduced after VA loading. VA loading with $\lambda = 0.75$ and $\lambda = 1$ resulted in some reduction of residual stresses. For $\lambda = 1.25$ a complete reduction of all beneficial compressive stresses after HFMI treatment occurs. Additionally, the first load cycle causes the majority of the stress redistribution. However, some additional yielding is observed during the second load cycles for the higher VA loads. Increasing the number of cycles above two does not seem to have any significant impact on the

final stress state. Closer examination of the stress-strain development for the different load cases would be recommended to further understand the effect of cycle count.

4 Discussion

As the project was run in a progressive manner divided into three stages, the results are presented, discussed, and conclusions are drawn after each stage in order for the subsequent stage to benefit from the conclusions. The main discussion points of each stage are summarised and extended here. Furthermore, error sources are presented.

4.1 Discussion regarding Stage 1

Convergence problems were encountered when using MSIS with cylindrical indenter tools. To facilitate convergence for 4PMSIS-seq, the edges of the cylinder were rounded with a radius of 2 mm, while the flat part of the cylinder was kept at 2.5 mm, resulting in a pellet shaped geometry for the indenter tool, as shown in Figure 22. This greatly decreased the total CPU time needed to run the simulations.

The quasi-static 4PMSIS-seq Chaboche gave the best results in the residual stress comparison, although it required fairly high computational effort. The 4PMSIS-seq does also leave an irregular stress profile, meaning that it could be unreliable for practical application. The 1PSIS dynamic explicit had the least computational effort. However, since the proper procedure time for the loading could not be implemented, some uncertainty of the result still remains. 1PSIS quasi-static gave the second best results with respect to computational effort and also gave comparable results.

The Chaboche mixed material model was favoured in Stage 1 and its use was continued in Stage 2 and 3. However, one flaw with the used model is that there exists no temperature-dependent material data, making the residual stresses from the weld treatment impossible to simulate for future work.

4.2 Discussion regarding Stage 2

In Stage 2, Section 3.2, it was established that the residual stresses from a majority of indenter tool models were quite similar. However, some models produced unexpected and questionable results. First, 5PAMSIS-mir failed to establish compressive residual stresses in the transverse direction. This is somewhat counterintuitive to the concept of compressive stresses forming when applying a compressive load. However, as the given problem is three-dimensional, additional factors might influence these results. Second, 4PASIS and 5PAMSIS-mir exhibit an opposing trend as compared to other simulations for transverse residual stresses along Path B. The reason behind this disparity is currently unknown. However, possible explanations could be linked to the indentation direction of the angled corner sections, which is not perpendicular to the weld at the weld toe node. Furthermore, the validity of comparisons between data from simulations and results from [1] should be examined. A completely fair comparison cannot be made as the data from [1] were produced by combining data from two separate simulations.

4.3 Discussion regarding Stage 3

As in Stage 2, a boundary condition prevents all nodes in the lower surface of the coupon from translating in the through-thickness direction. In the HFMI simulations of the previous stage, it is reasonable to assume that this type of motion is restricted since the specimen will likely be supported by a table or other flat surface from below. The situation which the cyclic loading is supposed to mimic is such that the coupon will be attached at its ends as part of a mechanical structure, and the motion of the lower surface will therefore not be restricted in the through-thickness direction, as opposed to during HFMI treatment. The stiffener causes an asymmetry with respect to the L-T plane, and the coupon will therefore tend to bend around the transverse axis during loading in the longitudinal direction. However, since bending is prevented by the boundary condition, the results regarding stresses and deformations are affected. The effect was assumed to be negligible, but simulations with other sets of boundary conditions would be beneficial to determine if this assumption is valid.

The results in Figure 21 was compared to the experimental data [5] originates from measurements on a actual physical coupon. Since this coupon was welded, there were residual stresses and metallurgical changes from the welding before commencing HFMI treatment. To compensate for this in regard to residual stresses, the redistribution of residual stress because of cyclic loading was examined, instead of studying absolute values of stress. By doing this, it was assumed that the data was comparable, but to which extent this is true is not entirely known. The metallurgical changes were entirely disregarded.

4.4 Error sources

A number of potential error sources have been identified which may have affected the simulations or data processing, giving erroneous results.

4.4.1 Analysis type

The validity of the dynamic simulations has to be mentioned as the proper procedure time of 0.0005 s, corresponding to 100 Hz could not be implemented. Some elements distorted excessively, causing the simulations to fail. Time did not allow for this problem to be rectified. Instead a longer procedure time was chosen to circumvent this problem. It is likely that the results of the dynamic simulations are not entirely accurate as realistic dynamic effects were not fully implemented. The longer procedure time did however yield results similar to those of the quasi-static analysis.

4.4.2 Indenter tool model for cuboid case

Extensive efforts were made to get the MSIS-seq simulations to converge for the cuboid geometry with cylindrical tools similar to those shown in Figure 7. However, since convergence issues occurred, the geometry of the tool was modified and a radius of 2 mm was added to the sides of the cylinders creating a pellet shape, as shown in Figure 22. The flat part with contact to the surface was kept at 2.5 mm and the fillet edges simply intersected each other. It was thought that the rounded shape would better resemble the shape of the peening tool and that the results were good. However, the results for the MSIS-mir and SIS were done with the original, cylindrical design of the indenter tools and comparisons to MSIS-seq might not be completely fair.

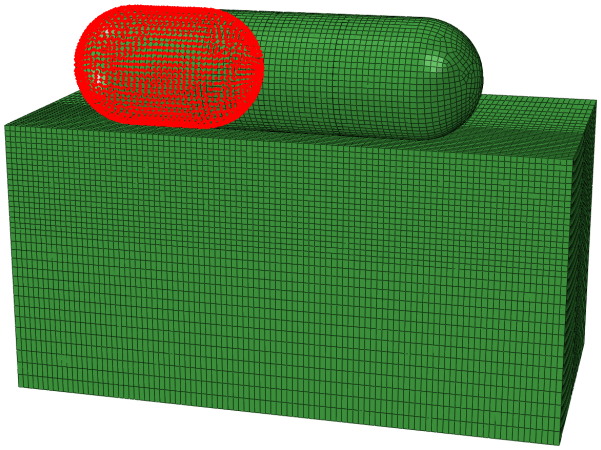

Figure 22: The tool geometry used for MSIS-seq with rounded edges of radius 2 mm with nodes of one tool shown in red

4.4.3 Coupon mesh

As mentioned in Section 2.2, there were some issues with the coupon model. As these issues were discovered after a majority of the simulations in Stage 2 had been run, the mesh with the erroneous elements was used throughout the stage in order to compare the results fairly. Therefore, there is an apparent risk that the results in Section 3.2 might be flawed. After the mesh was rectified the HFMI simulation with the final chosen indenter model was performed on the new mesh before the commencing Stage 3. To analyse the influence of the mesh, the final chosen indenter model was simulated with the rectified mesh and compared to the previous results, as shown in Figure 23. As can be seen, differences do appear between the different meshes. However, the differences are small and the results are overall very comparable.

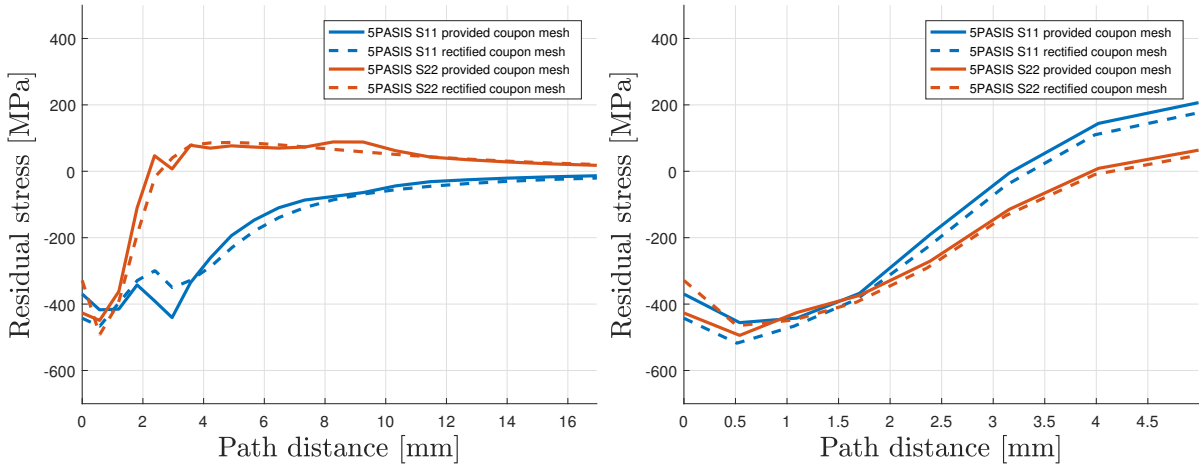

(a) Path A (b) Path B

Figure 23: Comparison between provided coupon mesh and rectified coupon mesh

Finite element analyses result in discrete fields of variables of interest, such as stress, defined in the mesh elements. In cases where variable values in nodal points or element boundaries are needed, such as when plotting the stresses along the Paths A and B, averaging of the variable values from the connected elements must be performed by ABAQUS. When extracting the stress-strain data seen in Figure 19b, this averaging process was investigated further by studying the original element values for the stress and strain. It came to the project group's attention that there are extremely large differences in the variable values for the different elements that are connected to the weld toe node. These large differences between adjacent elements might indicate that the elements are too large to accurately capture the stresses and strains in this region of high variable gradients. In order to make accurate assessments of stresses in the critical areas around the indentation path, a finer mesh is likely beneficial.

The coarseness of the mesh also seems to introduce stress concentrations where the elements connect to each other, as the coarseness creates angles in the interfaces between elements. This can be seen in Figure 24. Although this effect will be present even with a finer mesh, the angles between the surfaces of adjacent elements will be reduced if the number of elements is increased, reducing the magnitude of this error.

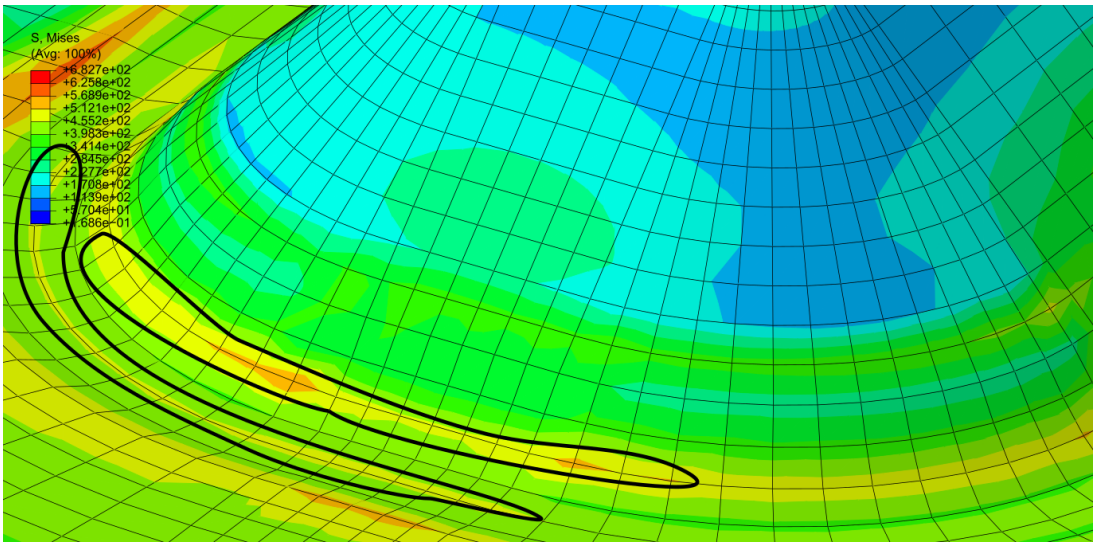

Figure 24: Stress concentrations due to mesh coarseness.

5 Conclusions and future work

The main goal of the project was to contribute to the ISSC 2018 benchmark on HFMI by documenting the effects of cyclic membrane loading on beneficial compressive residual stresses induced by HFMI. Conclusions regarding this goal follow:

- The redistribution of beneficial compressive residual stresses induced by HFMI is largely dependent of the peak load amplitude. With a larger peak load, more beneficial compressive residual stresses will be eliminated. A maximum peak load of $S_{\max} = \lambda/k_{\mathrm{t}} \cdot \sigma_{\mathrm{y}} = 0.78125\sigma_{\mathrm{y}}$ reduced the beneficial compressive residual stresses by almost 100 % whereas for $S_{\max} = \lambda/k_{\mathrm{t}} \cdot \sigma_{\mathrm{y}} = 0.6250\sigma_{\mathrm{y}}$ they were only reduced by 50 %. The implication of this is that when designing structural components and using HFMI to treat welds, unexpected peak loads must be considered as a single peak load can completely reduce the beneficial effects from HFMI.
- The majority of the redistribution of beneficial compressive residual stress occurs during the first load cycle. This agrees with previous works, e.g. [5].

The sub goal of the project was to obtain an indenter tool model, constitutive hardening model, and analysis type which yields comparable results to experiments without the use of excessive computational power. Conclusions regarding this goal follow:

- The friction coefficient for the tangential interaction between indenter tool and cube was found to not significantly impact the residual stresses.
- When considering the computational effort of simulating HFMI on the cuboid, SIS was found to be most favourable. This method proved to give comparable results to experimental work, e.g. [3, 6], at least in the region close to the surface ($< 2\,\mathrm{mm}$).
- Simulations on the cuboid model showed that the Chaboche hardening model consistently gave comparable results. The choice of material model was also influenced by the considerable variance in the residual stress state by the choice of data points used from Table 2 for isotropic and kinematic hardening.
- At this time no final recommendation can be given to which analysis type should be used, because of the aforementioned concerns with the the dynamic simulations. However, from Table 3 of the computational effort it is noted that the dynamic explicit analysis shows great potential.
- From simulations performed on the coupon model it was concluded that SIS gives comparable results for longitudinal residual stresses regardless of number of parts or indentation angle. Furthermore, MSIS proved to provide unreliable results for both longitudinal and transverse residual stresses.

Future work is required for simulations of MSIS. Unfortunately, time did not permit evaluation of different material models or analysis types for this indenter tool model. Considering the result of MSIS-seq in Figures 8c and 8d, it would be of interest to investigate if even more accurate results could be obtained for MSIS-seq. An investigation of why the CPU time needed to simulate the indentations with a cylindrical geometry was much higher than for the pellet shaped geometry would also be of interest to conduct.

Furthermore, it is recommended to perform further simulations using kinematic and isotropic hardening as the temperature-dependent material properties that are needed to implement the Chaboche material model in welding simulations do not exist.

Additionally, it is recommended that further investigation of the dynamic simulations are carried out to obtain comparable results with the proper procedure time. Especially the dynamic explicit, as simulations ran with very low computational effort.

To achieve a better understanding of the effects of cyclic loading, it is recommended to study the results from a wider range of load amplitudes, as well as the effects of peak loads in different positions in regard to CA loading. It would also be valuable to do a more detailed investigation of the stress-strain development during this loading, to further validate and extend the current findings, which indicate that most of the impact from cyclic loading occurs in the first one or two cycles. The choice of sample points to determine stresses in nodes also seems to be of significance. Future study of this, and other mesh parameters such as coarseness, would be interesting.

References

[1] L. Josefson, J. Alm, and J.M.J. McDill. "Simplified FEA models in the analysis of the redistribution of beneficial compressive stresses in welds during cyclic loading". In: *Proceedings of the 37th International Conference on Ocean, Offshore and Arctic Engineering*. 2017-06-22, Madrid, Spain. 2017.

[2] J. Alm et al. *Fatigue Life Improvement of Welded Joints, TME131 Project in Applied Mechanics*. Chalmers University of Technology, Gothenburg, Sweden. 2017.

[3] L. Josefson et al. *Committee V.3 - Materials and Fabrication Technology in Proceedings of the 20th International Ship and Offshore Structures Congress (ISSC 2018)*. Editors: Kaminski, M. and Rigo, P., in Liege, Belgium and Egmond aan Zee. The Netherlands, September 9-14.

[4] E. Harati et al. "Effect of HFMI treatment procedure on weld toe geometry and fatigue properties of high strength steel welds". In: *Procedia Structural Integrity* 2 (2016), pp. 3483–3490.

[5] M Leitner et al. "Fatigue strength of welded and high frequency mechanical impact (HFMI) post-treated steel joints under constant and variable amplitude loading". In: *Engineering Structures* 163 (2018), pp. 215–223.

[6] J. Foehrenbach, V. Hardenacke, and M. Farajian. "High frequency mechanical impact treatment (HFMI) for the fatigue improvement: numerical and experimental investigations to describe the condition in the surface layer". In: *Welding in the World* 60.4 (July 2016), pp. 749–755. ISSN: 1878-6669. DOI: 10.1007/s40194-016-0338-4. URL: https://doi.org/10.1007/s40194-016-0338-4.

[7] C3SE - Chalmers Centre for Computational Science and Engineering. https://www.c3se.chalmers.se/. (Accessed: 2018-05-15).

[8] Dassault Systemes - ABAQUS/CAE, version 6.14.2. https://www.3ds.com/se/produkter-och-tjaenster/simulia/produkter/abaqus/. Accessed: 2018-03-27.

[9] Abaqus 6.14 - Documentation. http://abaqus.software.polimi.it/v6.14/index.html. Accessed: 2018-05-11.

[10] K. Hemmesi, M. Farajian, and M. Boin. "Numerical studies of welding residual stresses in tubular joints and experimental validations by means of x-ray and neutron diffraction analysis". In: *Materials & Design* 126 (2017), pp. 339–350.

[11] R.V. Milligan, W.H. Koo, and T.E. Davidson. "The Bauschinger effect in a high-strength steel". In: *Journal of Basic Engineering* 88.2 (1966), pp. 480–488.

[12] Dassault Systemes - CATIA V5. https://academy.3ds.com/en/software/catia-v5-student-edition. Accessed: 2018-03-27.

[13] L. Josefsson. *Personal communication*. 2018-03-20, Gothenburg. 2018.